A Comparison of Forward-Boundary-Integral and Parabolic-Wave-Equation Propagation Models

C. L. Rino, *Fellow, IEEE,* and Valerie R. Kruger

***Abstract*—The parabolic wave equation and its variants have provided the theoretical framework for most practical forward-propagation models. Split-step integration generates an easily obtained, robust solution for most applications. Irregular boundaries can be incorporated by using a conformal mapping technique introduced by Beilis and Tappert [1] and refined by Donohue and Kuttler [2]. In an earlier paper, we demonstrated an alternative method that incorporates a numerical solution to the forward boundary-integral equation within each split-step cycle [3]. This paper compares predictions of forward propagation obtained by these two distinctly different methods. The results confirm that the PWE-based method is very accurate for smoothly varying surfaces and that it captures the primary forward structure even in the presence of unresolved surface detail. The moderate loss of fidelity is often an acceptable trade for for increased computational efficiency. There are situations, however, where the details of the surface structure are important. Furthermore, the induced surface currents are unique to the forward boundary-integral method. We illustrate their use by calculating the bistatic scatter that would be measured from an isolated surface segment. We show that the scattered field measured in this way can be normalized to form a bistatic scatter function only when the illuminating beam is tilted slightly toward the surface. We interpret this disparity as a breakdown in concept that underlies a local scattering function.**

***Index Terms*—Propagation, scattering.**

I. Introduction

WAVE propagation in an unbounded weakly inhomogeneous medium can be characterized by coupled first-order differential equations that are structurally similar to transmission-line or waveguide mode equations. The coupled equations individually characterize the forward-propagating (away from the source) and the backward-propagating (toward the source) components of the total field, although the forward component typically carries most of the energy. The forward approximation exploits this asymmetry by neglecting the backward-propagating component in the forward equation. The parabolic wave equation (PWE) and its variants are well-known applications of the forward approximation. Their broad appeal is largely attributable to a robust split-step recursion that generates practical solutions for most applications. Plane reflecting boundaries are readily incorporated in the split-step framework, but irregular surfaces present a formidable challenge.

The theory of scattering from irregular surfaces requires the computationally demanding solution of an intermediate boundary integral equation (BIE). Although a transmission-line formulation of the surface-scattering problem has been known for some time [4], methods that exploit that structure have been introduced only recently by Holliday *et al.* [5] and by Kapp and Brown [6]. Scattering theory has focused mainly on methods that use recursive aggregation of scattering centers with translation to a common reference [7], although a variant of the forward approximation has been used to reduce the computation burden of the fast BIE solvers [8]. Chou and Johnson [9] used the scheme in the forward–backward method of Holliday *et al.* [5] to adapt BIE solvers for large-scale problems, but accommodating varying refractivity in a BIE framework has been addressed only for special cases [10]. Thus, BIE methods have remained largely outside the domain of practical forward-propagation models.

Irregular boundaries are incorporated in PWE-based models in a totally different way. Donohue and Kuttler [2] refined a method developed originally by Beilis and Tappert [1], but first applied to microwave propagation models by Barrios [11]. The Beilis–Tappert scheme effectively transforms the surface structure into a phase perturbation that is added to the refractivity component. The manipulations require no significant increase in computational complexity, but the approximations used to reformulate the transformed propagation equations impose some restrictions. Finite difference methods also have been used effectively to accommodate irregular boundaries in forward-propagation computations [12], [13].

We show in this paper that, under the forward approximation, irregular surfaces can be accommodated in a split-step algorithm at the same level of fidelity as the finite-difference methods. The forward approximation allows redefinition of the total field as a new source, whereby the propagation medium can be incorporated in the same way that it is incorporated in the PWE split-step algorithms. Field redefinition also improves the efficiency of the forward BIE solution by reducing the number of Bessel function evaluations. To demonstrate PWE-BIE tradeoffs, we compare propagation predictions from our BIE method as described in Rino and Ngo [3] and a simplified implementation of the scheme described by Donohue and Kuttler. As it happens, a simplified form of their linear shift map is intrinsically part of the forward-BIE computation.

Our results support the postulate that PWE-based methods capture the essential characteristics of scatter from a surface smooth on the scale of the forward-marching integration step. Our method is very efficient for what it achieves, but it does require substantially more computation than PWE. Beyond generating fine structure in the forward fields, however, the BIE method produces surface currents that can be used to approximate bistatic scatter as would be measured, for example, by

Manuscript received June 17, 1999; revised June 1, 2000. This work was supported by the Naval Surface Weapons Center under Contract N00178-97-C-3085 and by Vista Research internal funds.

The authors are with Vista Research, Inc., Sunnyvale, CA 94086 USA.

Publisher Item Identifier S 0018-926X(01)01276-5.

remotely sensing the scatter from an isolated surface segment. The PWE field near the surface is sometimes used as an input to a specified surface scattering function to approximate average bistatic scatter, whereas surface currents provide problem-specific information and practical bounds on the use of local bistatic scattering functions.

II. Background

Wave propagation is governed by Helmholtz' equation, which we write here as

$$\nabla^2\psi(\overline{r})+k^2\psi(\overline{r})=-S(\overline{r}). \tag{1}$$

Hereafter, an overbar will be used to denote a vector. The three-dimensional (3-D) complex scalar field $\psi(\overline{r})$ has the implicit temporal variation $\exp\{2\pi ift\}$, and $k=2\pi f/c$ where c is the propagation velocity in the homogeneous background medium. In the absence of boundaries, (1) admits the formal solution

$$\psi(\overline{r})=\psi_0(\overline{r})+\iiint S(\overline{r}\,')G(\overline{r},\overline{r}\,')\,d\overline{r}\,' \tag{2}$$

where $G(\overline{r},\overline{r}\,')=\exp\{ik|\overline{r}-\overline{r}\,'|\}/4\pi|\overline{r}-\overline{r}\,'|$ is the free-space Green function, and $\psi_0(\overline{r})$ is a solution to the homogeneous form of (1). Weak inhomogeneities are introduced by using the source function

$$S(\overline{r})=2k^2\delta n(\overline{r})\psi(\overline{r}) \tag{3}$$

where $\delta n(\overline{r})$ is the perturbation to the refractive index $n=c_0/c$, and c_0 is the reference (acoustics) or vacuum velocity (electromagnetics).

Elaborating on our earlier development [3], it can be shown that the two-dimensional (2-D) Fourier decomposition of (2) in the yz plane at x can be separated into forward- and backward-propagating field components as follows:

$$\hat{\psi}^+(x;\overline{K})=\hat{\psi}_0(x;\overline{K})+\int_0^x \hat{S}(x';\overline{K})\times\frac{i\exp\{ik_x(K)(x-x')\}}{2k_x(K)}\,dx' \tag{4}$$

$$\hat{\psi}^-(x;\overline{K})=\int_x^L \hat{S}(x';\overline{K})\,\frac{i\exp\{-ik_x(K)(x-x')\}}{2k_x(K)}\,dx' \tag{5}$$

where $\overline{K}$ is the 2-D transverse wavevector, and $k_x(K)=\sqrt{k^2-K^2}$. The total field is obtained by the superposition

$$\psi(x,\overline{\rho})=\psi^+(x,\overline{\rho})+\psi^-(x,\overline{\rho}) \tag{6}$$

where $\overline{\rho}=(y,z)$. Differentiating the defining equations with respect to x yields the coupled first-order differential equations

$$\pm\frac{\partial\hat{\psi}^{\pm}(x;\overline{K})}{\partial x}=ik_x(K)\hat{\psi}^{\pm}(x;\overline{K})+\frac{i\hat{S}(x;\overline{K})}{2k_x(K)}. \tag{7}$$

Substituting from (3) and transforming back to the spatial domain recasts the equations in their spatial-domain form

$$\pm\frac{\partial\psi^{\pm}(x,\overline{\rho})}{\partial x}=ikQ\psi^{\pm}(x,\overline{\rho})+2k^2\iint G(k|\overline{\rho}-\overline{\rho}\,'|)\times\delta n(x,\overline{\rho}\,')\psi(x,\overline{\rho}\,')\,d\overline{\rho}\,'. \tag{8}$$

The propagation operator

$$Q\equiv\sqrt{1+\frac{1}{k^2}\nabla_\perp^2}\Leftrightarrow\sqrt{1-\frac{K^2}{k^2}} \tag{9}$$

is defined by expanding the square root in a Taylor series with the term containing the transverse Laplacian ($\nabla_\perp=\partial/\partial y+\partial/\partial z$) used in place of the expansion variable. The formal equivalence implied by (9) can be established by a term-by-term association with the Taylor series expansion of the exponential propagation factor in the homogeneous solution to (7).

If only the $\overline{K}=0$ mode survives, with $S=0$, (7) reduces to the ordinary transmission-line equations. The source function can be configured to represent small nonuniformities in the characteristic impedance. Up to this point, however, no approximations have been made beyond those implicit in (3). Moreover, the equations are equally valid for principal propagation perpendicular or parallel to the surface reference plane. For perpendicular propagation the x axis is vertical, and the model can be used to generate transparent boundary conditions essentially equivalent to those demonstrated by Levy [14], [15]. For horizontal propagation, the integral term in (8) can be simplified by noting that $G(k|\Delta\overline{\rho}|)$ decays rapidly compared to the scale of change of the remaining factors in the integrand. Removing these terms and integrating the Green functions shows that

$$2k^3\iint G(k|\Delta\overline{\rho}|)\delta n(x,\overline{\rho}\,')\psi(x,\overline{\rho}\,')\,d\overline{\rho}\,'\approx ik\delta n(x,\overline{\rho})\psi(x,\overline{\rho}) \tag{10}$$

which is the familiar phase perturbation that appears in the PWE.

With or without approximation to the media-interaction term, the form of (8) suggests the forward approximation $\psi(x,\overline{\rho})=\psi^+(x,\overline{\rho})$, which leads to the forward-propagation model basic to this paper and the PWE-based methods in general

$$\frac{\partial\psi^+(x,\overline{\rho})}{\partial x}=ikQ\psi^+(x,\overline{\rho})+ik\delta n(x,\overline{\rho})\psi^+(x,\overline{\rho}). \tag{11}$$

Because the free-space propagator $\exp\{ik_x(K)x\}$ is a symmetric function of K_z, propagating the antisymmetric or the symmetric extensions of $\psi(x,\overline{\rho})$ preserves that symmetry with respect to x. If there are no y variations, these modes satisfy the canonical boundary conditions for impenetrable surfaces. For weakly penetrable surfaces, one can use an impedance boundary condition, which is a linear combination of the normal derivative and complex field on the surface. Kuttler and Dockery [16], [17] developed a mixed Fourier transform that satisfies both (11) and the impedance boundary condition for a flat surface.

For an irregular boundary, surface height is a function of position, $z=f(x,y)$. Beilis and Tappert [1] introduced the transformation

$$\tilde{x}=x,\quad \tilde{y}=y,\quad \eta=z-f(x,y) \tag{12}$$

which effectively replaces the original x and y derivatives by

$$\frac{\partial}{\partial x,y}<=\frac{\partial}{\partial\tilde{x},\tilde{y}}-f_{x,y}(\tilde{x},\tilde{y})\,\frac{\partial}{\partial\eta}. \tag{13}$$

The transformation changes the form of the original equations, but the distortions can be overcome by introducing an appropriately chosen phase function and making some additional approximations. Donohue and Kuttler [2] developed a refined version of this scheme that effectively replaces the stair-step approximation with linear segments and incorporates the mixed Fourier transformation. They introduced the term linear shift map (LSM) to describe the refined method. To distinguish that method from our own procedure described below, we will use the term "simplified" linear shift map (SLSM).

In the SLSM coordinates, the free-space propagator becomes

$$\psi(\tilde{x},\tilde{y},\eta) = \iint \hat{\psi}(0;\overline{K})\exp\{i(k_x(K)\tilde{x}+K_z f(\tilde{x},\tilde{y}))\} \times \exp\{i(\overline{K}\cdot\tilde{\rho})\}\frac{d\overline{K}}{(2\pi)^2} \tag{14}$$

where $\tilde{\rho}=(\tilde{y},\eta)$. We convert this equation to a first-order differential equation by performing a perturbation expansion about $\tilde{x}$ and taking the limits that define the partial derivative of ψ with respect to $\tilde{x}$. The result is

$$\frac{\partial\psi}{\partial\tilde{x}} = \iint i(k_x(K)+K_z f_x(\tilde{x},\tilde{y}))\exp\{iK_z f(0,\tilde{y})\}\hat{\psi}(0;\overline{K}) \times \exp\{i\overline{K}\cdot\tilde{\rho}\}\frac{d\overline{K}}{(2\pi)^2}. \tag{15}$$

Because of the $\tilde{y}$ dependence of $f_x(\tilde{x},\tilde{y})$, Fourier transformation in the shifted coordinates is possible only for a one-dimensional surface, whereupon

$$\frac{\partial\hat{\psi}(\tilde{x};K_z)}{\partial\tilde{x}} = i(k_x(K)+K_z f_x(\tilde{x}))\hat{\psi}(\tilde{x};K_z). \tag{16}$$

Equation (16) shows that propagation in the SLSM system can be achieved by adding the term $K_z f_x(\tilde{x})$ to the wide-angle propagation operator. It follows that, to the extent that the surface can be approximated by piecewise horizontal segments, all the previous methods can be generalized by using (16) in place of the propagation operator. No further manipulation of the equations is necessary.

III. Boundary Integral Equation Methods

Any solution to the Helmholtz equation can be represented as a superposition of radiating elements on a surface that isolates the field sources. Boundary integral equations uniquely determine induced sources that support the scattered field (see, for example, [18, Ch. 8.3]). Only the Dirichlet problem for a one-dimensional surface (zero field on the surface) will be developed here, although the method is restricted only by the forward approximation. The BIE method for a one-dimensional surface is described in an earlier paper and the references cited therein [3]. For a field initiated at $x=x_0$, the continuous form of the BIE for the Dirichlet problem is

$$\frac{\partial\psi(x,f(x))}{\partial N} = 2\frac{\partial\psi_i(x,f(x))}{\partial N} - \frac{i}{2}\int_{x_0}^{\infty}\frac{\partial H_0^{(1)}(k\Delta\rho)}{\partial N} \times \frac{\partial\psi(x',f(x'))}{\partial N}\,dx' \tag{17}$$

where $\psi_i(x,f(x))$ represents the incident field propagated freely to the surface, $H_0^{(1)}(k\Delta\rho)$ is an outward radiating Hankel function of order zero, and

$$\partial\psi(x,z)/\partial N = \partial\psi(x,z)/\partial z - \partial f(x)/\partial x\partial\psi(x,z)/\partial x \tag{18}$$

is the unnormalized form of the normal derivative. In an electromagnetics problem, the normal derivative of the horizontal electric field is proportional to the magnetic field, whereby the source is effectively an electric sheet current.

To solve (17) numerically, it is necessary to obtain a discrete approximation to the unknowns. However this is done, the result is a system of linear equations with unknowns that define the source function. The forward approximation amounts to truncating the integration in (17) at x. Point-matching produces the following system of equations

$$\frac{\partial S^{(0)}(x_j)}{\partial N} = 2\frac{\partial S_i(x_j)}{\partial N} - 2\sum_{l=1}^{j-1}M_{jl}\frac{\partial S^{(0)}(x_l)}{\partial N} - 2M_{jj}\frac{\partial S^{(0)}(x_j)}{\partial N} \tag{19}$$

where $S(x_j)=\psi(x_j,f(x_j))$ with

$$M_{jl} = \begin{cases} \dfrac{ik_0^2}{2}\dfrac{H_1^{(1)}(k\Delta\rho_{jl})}{k\Delta\rho_{jl}}\xi_{jl}, & \text{for } j\neq l \\ \dfrac{\partial^2 f_j/\partial x^2}{1+(\partial f_j/\partial x)^2}\dfrac{\Delta x}{4\pi}, & \text{for } j=l \end{cases} \tag{20}$$

$$\xi_{jl} = [(f(x_j)-f(x_l))-(x_j-x_l)\partial f_j/\partial x]\Delta x \tag{21}$$

and

$$\delta\rho_{jl} = \sqrt{(x_j-x_l)^2+(f(x_j)-f(x_l))^2}. \tag{22}$$

The zero superscript indicates the lowest order approximation that would formally initiate the forward–backward method [5] or the method of ordered multiple interactions [6]. The solution is obtained by the forward recursion

$$\frac{\partial S^{(0)}(x_j)}{\partial N} = \frac{\partial S_i(x_j)/\partial N - \sum_{l=1}^{j-1}M_{jl}\partial S^{(0)}(x_l)/\partial N}{1/2+M_{jj}}. \tag{23}$$

The BIE solution and subsequent field reconstruction as described up to this point would be highly inefficient for a large-scale problem because resummation from x_0 is required for each new point. Clearly, one would like to aggregate the effects of the remote scatterers to carry forward only the essential information. This can be achieved by redefining the source field as follows:

$$S_m^{(0)}(x_{mM},z) = \psi_{m-1}^{(0)}(x_{mM},z) - \frac{i}{4}\sum_{l=(m-1)M}^{mM-1}H_0^{(1)}(k\Delta\rho_l) \times \frac{\partial S^{(0)}(x_l)}{\partial N}\,dx. \tag{24}$$

The notation $\psi_{m-1}^{(0)}(x_{mM},z)$ means the total field in the z plane at $x_{mM}=x(mM\delta x)$, which combines the previous total component propagated freely from $x_{(m-1)M}$ with the contributions from all the induced sources up to the source at x_{mM} whose

contribution is reduced by half. This minimizes a small transient that can be observed in source function near the redefinition point. With M the number of fine steps per field redefinition, the equivalent PWE sampling interval would be $M\Delta x$. With field redefinition, (23) becomes

$$\frac{\partial S^{(0)}(x_j)}{\partial N} = \frac{\partial S^{(0)}_{m-1}(x_j)/\partial N - \sum_{l=(m-1)M}^{j-1} M_{jl}\partial S^{(0)}(x_l)/\partial N}{1/2 + M_{jj}} \quad (25)$$

which together with (24) defines a forward-marching recursion.

It remains to describe the method of computing the excitation field on the surface. Let $\psi_m(x_j, \eta)$ represent the field at x_j in SLSM coordinates. From (14), it follows that

$$\begin{aligned}\psi_m(x_j,\eta) = \int \hat{\psi}_m\left(x_{(m-1)M}; K_z\right) &\times \exp\left\{iK_z\left(f(x_j) - f\left(x_{(m-1)M}\right)\right)\right\} \\ &\times \exp\{ik_x(K_z)(j-(m-1)M)\Delta x\} \\ &\times \exp\{iK_z\eta\}\, dK_z/(2\pi) \end{aligned} \quad (26)$$

where $\hat{\psi}_m(x_{mM}; K_z)$ is the Fourier transform in the SLSM coordinates. The normal derivative on the surface is obtained by taking $\eta = 0$. Computationally, this is achieved by shifting the phase to compensate for the height change in conjunction with the propagator. Thus, just one Fourier transform pair per cycle is required. Two additional vector multiplications per step generate $\partial S^{(0)}_{m-1}(x_j)/\partial N$. We see that calculating the field on the surface effectively introduces the SLSM in the BIE computation, but no approximation is involved. The final step in the compute cycle applies the phase perturbation $k\overline{\delta n}(x_{mM}, \eta)M\Delta x$ to the field defined by (24). The overbar denotes an average over the segment.

The additional computation over PWE includes the vector multiplications required to generate $\partial\psi^{(0)}_{m-1}(x_j)/\partial N$, the $M(M+1)/2$ evaluations of the Hankel function plus multiply-and-add computations required to evaluate (25), and the additional N_z evaluations required to redefine the source field per (24), where N_z is the number of z samples. A $2N_z$ point vertical FFT is common to both methods. In the field redefinition particularly, an asymptotic approximation to the Hankel function for large arguments significantly improves the efficiency of the computation. The recursion described by Chou and Johnson [9] could further improve computational efficiency in the evaluation of (25). CWAVE is a FORTRAN implementation of the forward BIE algorithm.

IV. Forward BIE-SLSM Comparisons

It is convenient to normalize the output from a forward-propagation model to the maximum far-field amplitude that could be delivered to the same far-field point in free space. By using the far-field form of $\psi(x, z)$, a propagation factor can be constructed as follows:

$$F(x,z) = \left|\frac{\psi(x,z)\sqrt{-2\pi ik\tilde{r}}}{\hat{\Psi}k\sin\theta_i}\right|^2 \quad (27)$$

where

- $\tilde{r}$ distance from the phase center of the source aperture;
- θ_i incidence angle from the z direction;
- $\hat{\Psi}$ integral of the amplitude distribution of the aperture field, which is the maximum field that could be delivered in the direction of $\tilde{r}$.

Our first example uses an extension of the raised sinusoid shown in [2, Fig. 2]. A 500-MHz CWAVE computation was initiated with a 3-m aperture field centered 50 m above the surface reference. The aperture field was tapered using a Hanning window. Propagation over a 9.8-km distance was simulated with 524 19.2-m split-step cycles. The propagator used a 2048-point FFT at two samples per wavelength. An exponential taper was initiated at 350 m above the surface to minimize reflections from the upper boundary. Within each split-step cycle, source fields were computed at 256 0.125-wavelength fine steps. A standard atmospheric profile supplies the refractivity variation, which is applied with height measured from the surface. The CWAVE computation required approximately 1 h on a 300-MHz pentium computer running Linux 4.2.

Fig. 1 shows the CWAVE propagation factor as a function of distance and height. The plot has been decimated to the display resolution. In the absence of focusing, the propagation factor achieves a maximum value of 4 (6 dB). The strong reflections on the facing side of the leading peak indicates an in-phase superposition of at least two of the interference peaks intercepting the lower portion of the profile. The fringing pattern on the facing side of the second profile peak is attributable to a similar interaction of the weaker field diffracted into the shadow of the first peak. Because the smooth profile generates no backscatter, forward BIE should capture all the scattering phenomena. Fig. 2 shows the same computation performed with a Matlab implementation of SLSM as defined by (16). To incorporate the Dirichlet boundary condition, the sine transformation pairs are used in place of the Fourier transform. For the SLSM computation, 50-m steps were used. The result shows that the simple interpretative Matlab implementation of SLSM, which executes in minutes, also captures the scattering phenomena albeit with some fine detail lost.

To demonstrate where significant departure between SLSM-PWE and forward-BIE calculations do occur, we used a wind-speed-dependent ocean surface-wave emulation to generate a random structure that is unresolved in the SLSM method. In fact, no attempt was made to introduce the fine structure into the SLSM computation since the increased sampling requirements defeat the purpose of using that approximation. The random field was superimposed on the raised sinusoidal profile creating a correlation scale of approximately 100 m. The CWAVE results are shown in Fig. 3. Comparison of Figs. 1 and 3 shows that the roughness scatters mainly at large scattering angles, with the primary forward field largely unaffected. To see this directly, the vertical profiles at 19.2 km are compared in Fig. 4. The smooth SLSM profile is denoted "0 mps," and the rough profile is denoted "6 mps," which is the wind speed used to generate the roughness component added to the smoothly varying surface profile. The differences are significant, although possibly acceptable as a speed-fidelity trade for many applications. Overall,

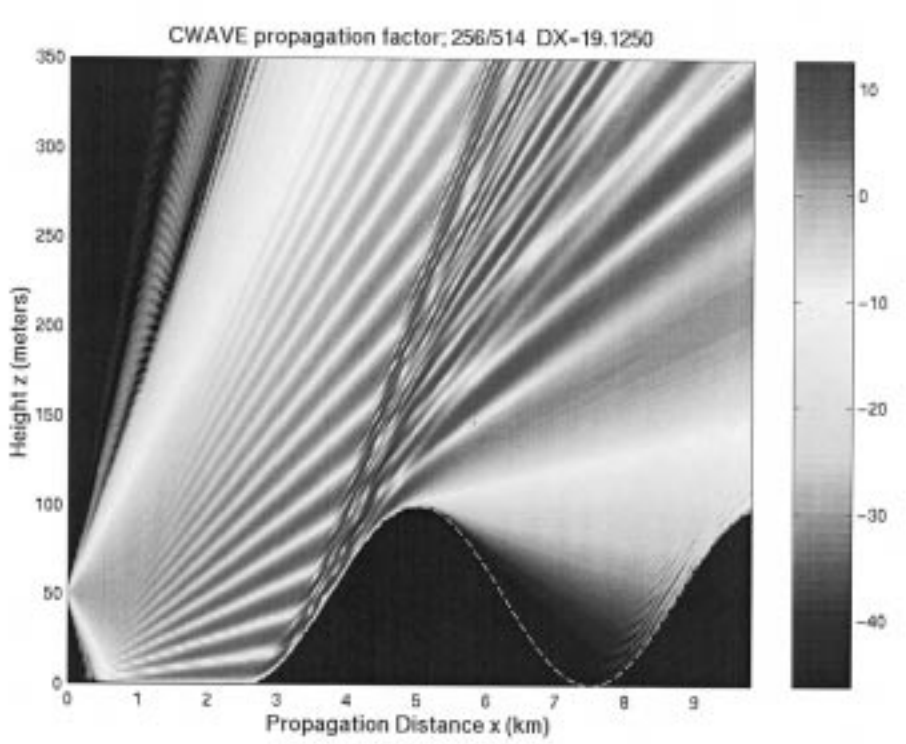

Fig. 1. CWAVE propagation-factor for 500-MHz source over large smooth sinusoidal obstruction. Focusing is observed on the facing side of the surface peaks.

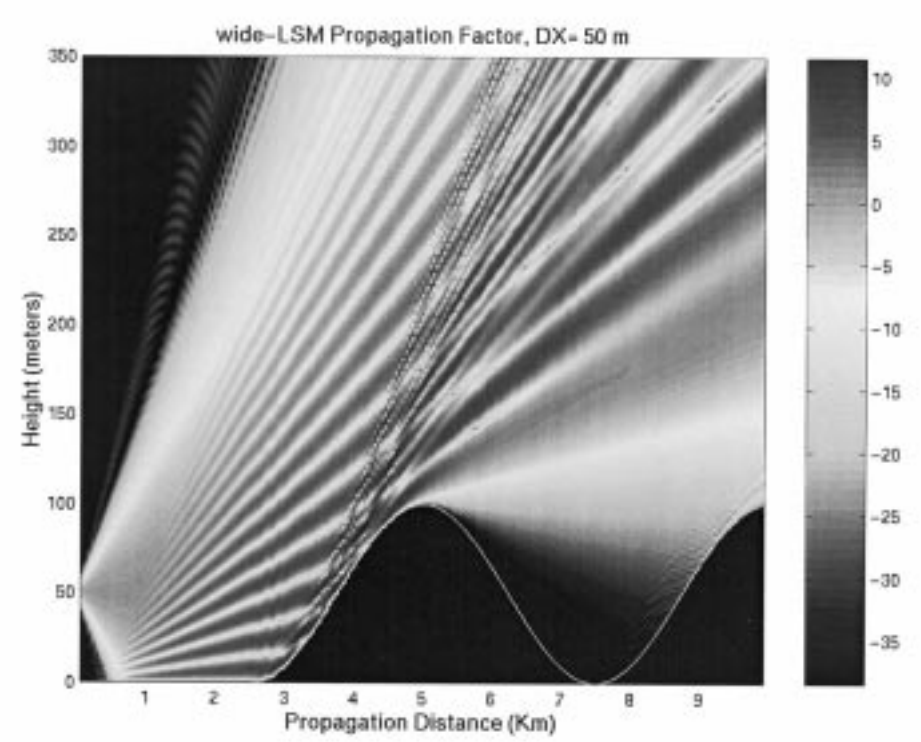

Fig. 2. Fourier-domain SLSM propagation factor for 500-MHz source with same propagation and surface conditions as shown in Fig. 1.

the SLSM method captures the essential characteristics surprisingly well.

The ramifications of nonspecular scatter in remote sensing presents a problem that cannot be addressed directly by using PWE-based methods because the surface structure must be known to calculate the backscatter. The two-scale model suggests simply applying the small-perturbation result with the calculated incident field. With the BIE method, this scheme can be tested directly. In a typical scenario, the transmit beam is pointed downward a few degrees or more to illuminate a

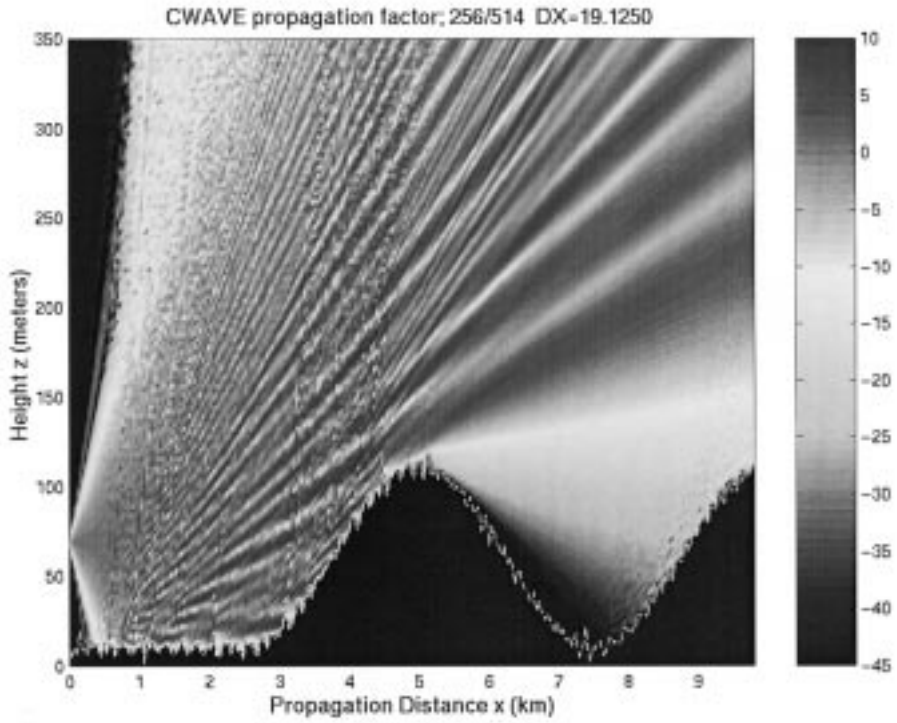

Fig. 3. CWAVE propagation factor for the same propagation environment shown in Fig. 1 but with small-scale surface-height variations added. The small-scale surface roughness scatters mainly at large angles.

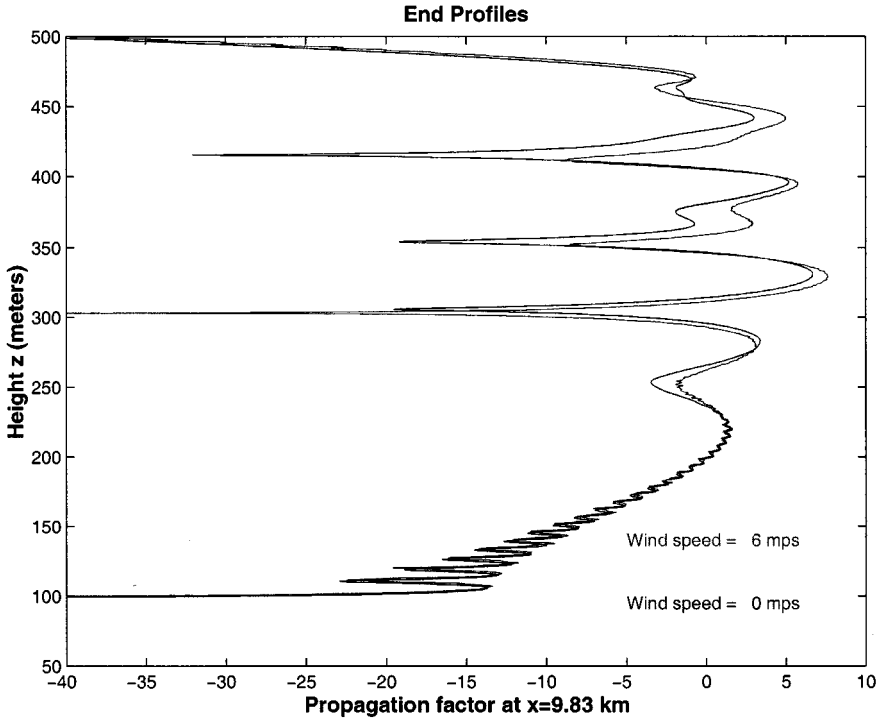

Fig. 4. Comparison of vertical profile at 19.2 km from the CWAVE computation shown in Fig. 3 with Fourier-domain SLSM emulation using the smooth surface. Wind speeds 6 mps and 0 mps refer to the bold and thin curves, respectively.

large surface segment. To simulate this situation, a "virtual" 1-GHz source was placed at a 50-m height above the surface. The actual source could be airborne at a much larger height and range. In the CWAVE computation, the aperture field is phased to point the beam 2.5° downward. The ocean surface generator was used to simulate structure representative of a 10-kt (5 m/s) wind. The frequency was increased to narrow the beam so that the phenomena of interest could be captured within a smaller computation range (256 cycles). Otherwise, the wavelength-normalized sampling was the same as used in the

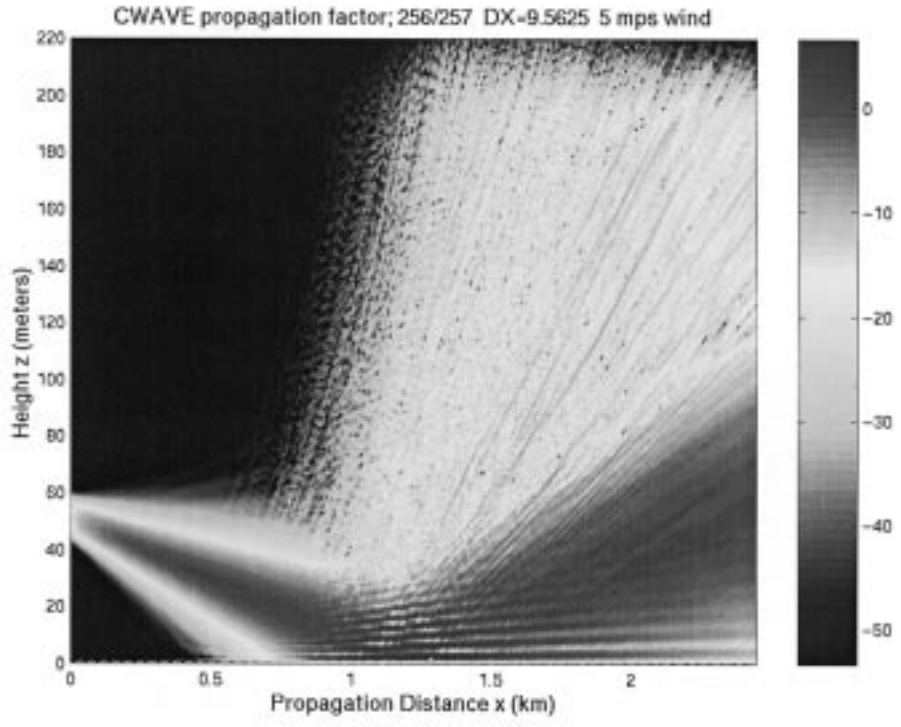

Fig. 5. CWAVE propagation factor for for 1-GHz source with a beam pointing 2.5° downward to reflect from rough ocean-like surface.

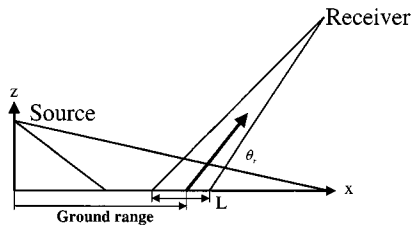

Fig. 6. Geometry for surface bistatic scatter computation.

previous examples. The CWAVE propagation factor is shown in Fig. 5. There is a substantial amount of nonspecular scatter that fills the region that would be devoid of scatter from a smooth surface. However, as with our previous experience, the specular forward beam is not too different from its smooth-surface reflection (not shown).

To pursue this further, we envision the experiment shown schematically in Fig. 6. An airborne radar receiver samples the scattered field by range gating the return pulse. To the extent that frequency dispersion is negligible over the frequency band, this isolates the surface scatterers to the projected range resolution on the surface. The currents within the range gate are influenced by scattering outside that window, but the isolation is modeled correctly within the limit of the forward approximation. The geometry defines a scattering angle θ_r from the center of segment of length L, which represents the projected range resolution defined by the difference in pathlength of the two rays shown in the figure. To calibrate such a measurement, it would be necessary to measure or calculate the power flux intercepting the isolated segment of the surface. In a numerical experiment, there is no impediment to perfect calibration. The scattered field was calculated over sliding segments as

$$\psi_s(x_j,\theta_r)=\frac{i}{4}\sum_{l=-(L-j)}^{L-j}H_0^{(1)}(k\Delta\rho_l)\,\frac{\partial\psi^{(0)}(x_l)}{\partial N}\,dx. \quad (28)$$

The bistatic scattering function referenced to the center of the sliding window is defined by the relation

$$\sigma/(4\pi\cos\theta_i)=k\cos^2\theta_r\left|\hat{\psi}(x:\theta_r)\right|^2/(2\pi I_i) \quad (29)$$

where I_i is the vertical flux crossing the surface. The integral of (29) over 2π rad should be unity, which is a good test of the consistency of both forward BIE and the construction of the bistatic scattering function.

The upper frame in Fig. 7 shows the forward bistatic scattering function as computed from (29) for a 500-m segment centered on the nominal specular reflection point, which is the unique point that satisfies Snell's law for the incident wave direction. The lower frame shows the agreement between the calculation of the total flux crossing a sliding 500-m surface segment centered on the ordinate (see Fig. 5) and the unnormalized bistatic scatter from the same segment, which should give the same value. As the incident grazing angle approaches zero, we observed that the surface segment required to achieve this level of agreement increases until it is no longer possible to obtain a consistent estimate of a bistatic scattering function. Effectively, a surface scattering function that is sensibly independent of the illuminating source cannot be constructed. Stated another way, at grazing incidence, the plane wave excitation that defines the scattering function is a mathematical construct that cannot be realized in an experiment. At low grazing angles, therefore, the full forward computation is necessary to calculate the surface scattering.

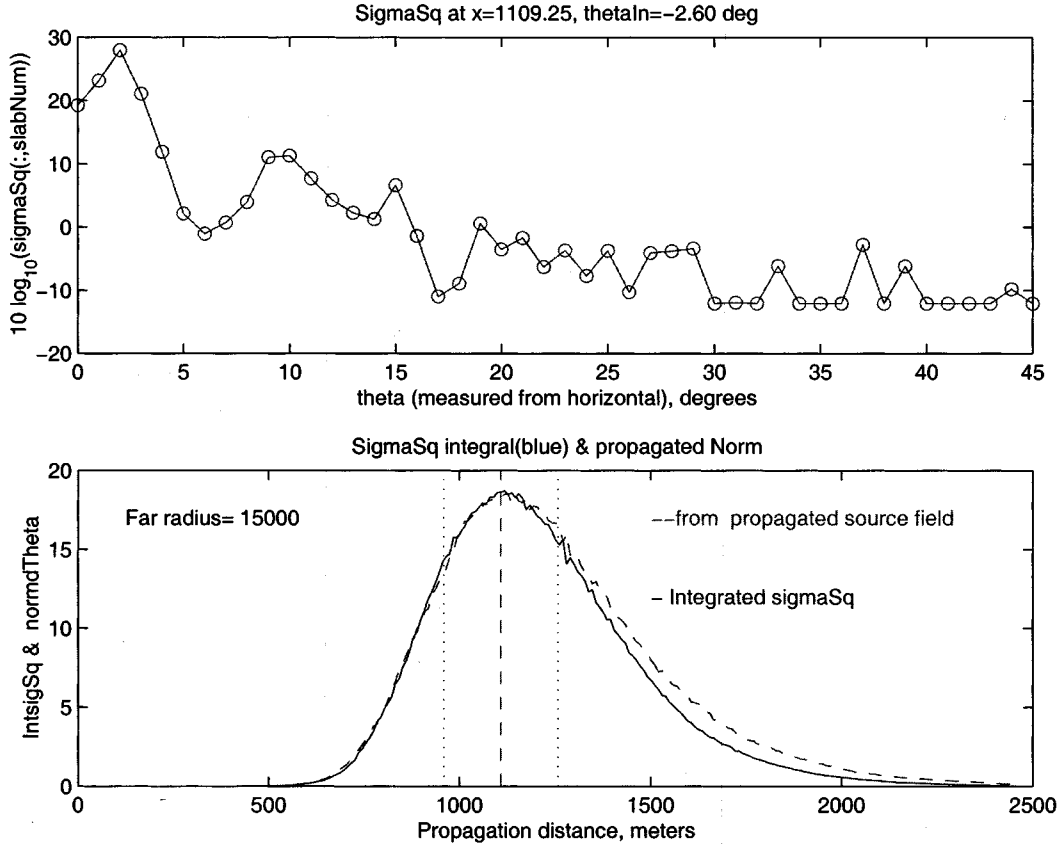

Fig. 7. Reconstruction of the bistatic scatter from a 500-m surface segment centered on nominal specular reflection point (upper frame) together with a direct and local computation of energy conservation for the scatter from a sliding surface segment (lower frame).

V. Discussion

In previous work, we demonstrated that the BIE formulation of surface scattering can be adapted for solution in a forward-marching algorithm that, with field redefinition, can accommodate a weakly inhomogeneous propagation medium. The scheme generalizes the PWE method, but to do so it is necessary to sample the surface at subwavelength intervals. The PWE methods typically sample the surface in steps of more than 100 wavelengths. They achieve their efficiency by using a coordinate system whose origin follows the surface. When Fourier-domain methods are used, the boundary conditions are strictly satisfied only on horizontal segments. Our SLSM scheme accepts the error introduced at the discontinuities. Donohue and Kuttler [2] adapted the method for piecewise linear segments, which strikes a compromise between exact local boundary conditions and edge effects. Results presented in this paper show that SLSM captures the principal scattering characteristics for a smoothly vary surfaces. However, the effects of small-scale random structure that would be unresolved with typical LSM or SLSM sampling are unique to the BIE method. Fig. 3 and particularly Fig. 5 show a clear separation in scattering angle of the two structure scales.

We also demonstrated that the source fields unique to the BIE method can be used to calculate the bistatic scatter from the surface directly. Our final example showed, however, that a consistent interpretation of the surface scatter as a local incremental phenomenon is possible only at grazing angles above at least one degree. In effect, a point is reached where the area necessary to resolve the grazing angle is too large to support a uniform incident field. In that situation, standard remote sensing methods must be replaced with a more complete forward scatter computations.

References

[1] A. Beilis and F. D. Tappert, "Coupled mode analysis of multiple rough surface scattering troposphere," *J. Acoust. Soc. Amer.*, vol. 66, pp. 811–826, 1979.

[2] D. J. Donohue and J. R. Kuttler, "Propagation modeling over terrain using the parabolic wave equation," *IEEE Trans. Antennas Propagat.*, vol. 48, pp. 260–277, Feb. 2000.

[3] C. L. Rino and H. D. Ngo, "Forward propagation in a half-space with and irregular boundary," *IEEE Trans. Antennas Propagat.*, vol. 45, pp. 1340–1347, Sept. 1997.

[4] R. E. Collin, "Electromagnetic scattering from perfectly conducting rough surfaces (a new full wave method)," *IEEE Trans. Antennas Propagat.*, vol. 40, pp. 1466–1477, Dec. 1993.

[5] D. Holliday, L. L. DeRaad, Jr., and G. J. St-Cyr, "Forward–backward: A new method for computing low-grazing angle scattering," *IEEE Trans. Antennas Propagat.*, vol. 44, pp. 722–729, May 1996.

[6] D. A. Kapp and G. S. Brown, "A new numerical method for rough-surface scattering calculations," *IEEE Trans. Antennas Propagat.*, vol. 44, pp. 711–721, May 1996.

[7] W. C. Chew and C.-C. Lu, "The use of huygens' equivalence principle for solving the volume integral equation of scattering," *IEEE Trans. Antennas Propagat.*, vol. 41, pp. 897–904, July 1993.

[8] R. J. Burkholder and D. H. Kwon, "High-frequency asymptotic acceleration of the fast multipole method," *Radio Science*, vol. 51, no. 5, pp. 1199–1206, May 1996.

[9] H.-T. Chou and J. T. Johnson, "A novel acceleration algorithm for the computation of scattering from rough surfaces with the forward–backward method," *Radio Science*, vol. 33, pp. 1277–1287, May 1998.
[10] R. Awadallah and G. S. Brown, "Electromagnetic wave scattering from a rough surface in a surface-based duct created by a linear-square refractive index profile," *IEEE Trans. Antennas Propagat.*, vol. 48, Oct. 2000.
[11] A. E. Barrios, "A terrain parabolic equation model for propagation in the troposphere," *IEEE Trans. Antennas Propagat.*, vol. 42, pp. 90–98, Jan. 1994.
[12] D. J. Thomson, "Wide-angle parabolic equation solutions to two range-dependent benchmark problems," *J. Acoust. Soc. Amer.*, vol. 87, pp. 1514–1520, 1990.
[13] M. D. Collins, "Higher-order parabolic approximations for accurate and stable elastic parabolic equations with application to interface wave propagtion," *J. Acoust. Soc. Amer.*, vol. 89, pp. 1050–1057, 1991.
[14] M. F. Levy, "Horizontal parabolic equation solution of radiowave propagation problems on large domains," *IEEE Trans. Antennas Propagat.*, vol. 41, pp. 137–144, Feb. 1995.
[15] ——, "Transparent boundary conditions for parabolic equation solutions of radiowave propagation problems," *IEEE Trans. Antennas Propagat.*, vol. 45, pp. 66–72, Jan. 1997.
[16] J. R. Kuttler and G. D. Dockery, "Theoretical description of the parabolic approximation/fourier split-step method of representing electromagnetic propagation in the troposphere," *Radio Science*, vol. 26, pp. 381–393, Feb. 1991.
[17] G. D. Dockery and J. R. Kuttler, "An improved impedance boundary algorithm for fourier split-step solutions of the parabolic wave equation," *IEEE Trans. Antennas Propagat.*, vol. 44, pp. 1592–1599, Dec. 1996.
[18] W. C. Chew, *Waves and Fields in Inhomogeneous Media*. New York: Van Nostrand Reinhold, Dec. 1990.

C. L. Rino (S'62–M'70–SM'83–F'89) received the B.S.E.E. and M.S.E.E. degrees from the University of California at Berkeley, in 1965 and 1966, respectively, and the Ph.D. degree in applied physics and computer science from the University of California at San Diego, in 1970.

From July 1970 to October 1987, he was with SRI International in Menlo Park, CA, as Staff Scientist and Assistant Director of the Radiophysics Laboratory. In 1987, he joined Vista Research, Inc., Sunnyvale, CA, where he is currently a Staff Scientist. Prior to joining Vista Research, he spent a year as Chief Scientist in the Radar and Propagation Effects Division of Mission Research Corp., Monterey, CA. He has published more than 50 scientific papers on optics, signal detection, ionospheric physics, propagation in random media, and electromagnetics. His main interests involve analysis of data from a variety of radio propagation experiments and radars that spawned a number of theoretical analyses of propagation and scattering in random media.

Valerie R. Kruger received the B.S.N.E. degree from the University of Wisconsin, Madison, and the M.S.N.E. and Ph.D. degrees from the University of California, Berkeley. She is a member of Sigma Xi and has worked with Vista Research, Inc. since 1996.